To be submitted to JoV

Structural variety of developing and equilibrium horizontal convection confined in a rectangular vessel resulting from different heating plate arrangements

T. Terada[1], D. Noto[2], Y. Tasaka[1,3*], T. Miyagoshi[3], T. Yanagisawa[3,1]

[1]Laboratory for Flow Control, Faculty of Engineering, Hokkaido University, Japan
[2]Department of Earth and Environmental Science, University of Pennsylvania, USA
[3]Japan Agency for Marine-Earth Science and Technology, Japan

Abstract

Flow structures formed in a rectangular fluid layer with an aspect ratio of four driven by a horizontal temperature gradient along the top boundary, so-called horizontal convection in both developing and equilibrium cases, were investigated via flow visualization using thermochromic liquid crystal microcapsules. Four separated heating panels on the top of the vessel allowed the influence of the heating plate arrangement on the determination of the flow structure to be examined. The velocity vector fields averaged in local space and time showed that the flow structures in the developing cases with an initial stable temperature stratification consisted of shallow circulation beneath the top boundary, with the time development of the structures being independent of the plate arrangement. The number of circulations along the top boundary is associated with locations having horizontal temperature gradients. In the equilibrium state, however, the flow structures are more complex because of the influence of the unstable temperature stratification, which is modified by the circulation.

Keywords: Horizontal convection, Thermochromic liquid crystal, Particle Tracking Velocimetry, Temperature field

1 Introduction

Thermal convection in fluid layers dominates large-scale fluid motion and therefore Rayleigh–Bénard convection (RBC), the thermal convection of a fluid layer heated from below and cooled at the top, has been investigated as the simplest model of such fluid motion. Over the long history of RBC studies, the influence of additional elements on the basic RBC, such as background rotation, magnetic field, heating/cooling configuration, etc., have been examined to approach more realistic phenomena. The influence of the temperature gradient along a common horizontal boundary is a typical element. This

* Corresponding author: ✉ tasaka@eng.hokudai.ac.jp

problem has often been considered when studying natural convective processes of land-sea-breeze circulation, heat- and cool-island circulation (Lu et al., 1997), and cross-shore circulation in littoral waters (Ulloa et al., 2022), as well as in industrial processes such as glass-melting furnaces (Gramberg et al. 2007; Chiu-Webster et al. 2008). In such cases, the baroclinic torque caused by a temperature gradient inclined with respect to the gravitational field affects the driving of the fluid layer and an overturning circulation dominating the entire fluid layer is formed; this effect is much weaker than buoyancy due to the unstable vertical temperature gradient in the thermal equilibrium state (Coman et al., 2006; Hughes & Griffiths, 2008).

In large-scale phenomena with long thermal diffusion time scales, such "horizontal convection," it is necessary to determine the dominance of the flow structure in transient states transitioning toward the equilibrium state (Mulllarney et al., 2004; Wang & Huang, 2005; Griffiths et al. 2013; Gayen et al., 2013). Most earlier studies on horizontal convection have considered equilibrium states, meaning that the system is thermally equilibrated with a thermal forcing at the common horizontal surface in a bounded domain; therefore, transient states have been less examined. Since Rossby (1965) experimentally confirmed scaling laws for global quantities in the equilibrium state, a large number of studies have suggested similar scaling laws defined by global parameters such as the Rayleigh number. Details concerning these discussions can be found in an extensive review by Hughes & Griffiths (2008) and references therein. In terms of transient states, Mori & Niino (2002) derived similarity solutions for developing horizontal convection with stable temperature stratifications for an unbounded fluid layer; they categorized the phenomena into three regimes depending on the initial stratification intensity and the elapse time. Noto et al. (2021) performed detailed experimental investigations of such phenomena in a rectangular vessel with an aspect ratio of four, uneven heating at the top boundary, and an initial stable stratification. They found that the overturning circulation dominating the whole horizontal extent emerges like the equilibrium states. It is, however, confined in a shallow region of the fluid layer beneath the heating surface and its thickness is dominated by the intensity of the stratification as defined by a dimensionless stratification parameter. The two states, transient and equilibrium, are physically connected and can be observed at the same configurations, but at different elapsed times from the initiation of thermal forcing. In the developing horizontal convection, the initial stable temperature stratification is relaxed with time, and the shallow single circulation becomes thicker. After a sufficiently long time, comparable to the thermal diffusion time scale or longer, the convection reaches a thermal equilibrium state, where the bulk temperature of the fluid layer corresponds to the mid-temperature of the heating boundary. The fluid layer therefore has a partially unstable stratification that induces a strong downward flow, and it is expected that the convection will then spread throughout the entire fluid layer.

In this fundamental configuration, in addition to the intensity of the temperature stratification and the horizontal temperature difference, there are many factors that need to be examined in the future,

e.g., the temperature distribution along the horizontal boundary and the aspect ratio of the vessel, to enable a more understanding of the phenomena in both states. Recent work by Reiter & Shishkina (2020) found good agreement in the Rayleigh number scaling for global quantities in a symmetrical system unlike that in classical horizontal convection. Details concerning flow structures realized with a variety of thermal forcing conditions, however, have not been discussed. The variety further recalls the issue of characteristic length scale describing the phenomena, which is a prescribed parameter in classical RBC as the thickness of the fluid layer, but not trivial in horizontal convections confined by a vessel with insufficient horizontal extent for the overturning circulation.

The experimental setup used in Noto et al. (2021) is capable of arranging heating sources by modifying temperature of four individual heating panels on top of the fluid layer. This allows various factors concerning such phenomena confined in closed vessels to be examined. In this paper, to study horizontal convection in closed vessels, we focus on the influence of the heating panel arrangement on determining the flow structures in both the transient and equilibrium states while maintaining the temperature difference along the top boundary. To distinguish instantaneous flow structures for the individual conditions, we qualitatively visualize the temperature field, and quantitatively visualize the velocity vector field adopting fine particle tracking velocimetry at a vertical cross-section of the quasi-two-dimensional convection cells. Following the introduction, the experimental setup and measurement techniques are summarized in Section 2. The flow structures in each case for different arrangements of the heating panels are explained in Section 3 by showing the flow field and supplementary movies of the instantaneous temperature fields. Finally, the conclusions of the study are given.

2 Experimental setup and procedure

A rectangular container with internal dimensions corresponding to a height of 50 mm (= L), a width of 200 mm ($4L$), and a depth of 50 mm (L), as used in our previous study (Noto et al. 2021), was adopted for the optical visualization of the horizontal convection (see the schematic diagram in **Fig. 1(a)**). The container is made of acrylic resin, which has smaller thermal conductivity, ~0.2 W/(m· K), than metals, $O(10^3)$ W/(m· K), with bottom and side wall thickness of 15 mm and 10 mm, respectively. The lid of the container is separated into four panels and each panel is made of a copper block including an inner cavity for water circulation from a thermostatic bath. Each of these panels has a horizontal length of L, which is a typical length scale in classical RBC studies. A larger number of panel divisions can be deduced from a combination of the preset result. The panels were insulated from each other by inserting a 4-mm-thick rubber sheet between them, and the temperature of the panels could be individually controlled. Further details concerning the setup are given in Noto et al. (2021).

The experiments were conducted under four types of boundary conditions, as schematically illustrated in **Fig. 1(b)**. Details concerning the types and set boundary temperature values are given in

Table 1. There are relatively low (denoted L) and high (denoted H) temperature panels (the temperature difference between the two is the same under every condition, $\Delta\theta = 2$°C), and the four characters in the "Arrangement" column in the table indicate the arrangement of the panels. For example, "HHLL" indicates that the two left panels have a higher temperature and the two right panels have a lower temperature. At all four conditions, both the developing and thermally equilibrated horizontal convection were realized. The test fluid was kept in the container with the room temperature controlled at $T_0 = 20$˚C as the initial temperature of the fluid layer. At $t = 0$, the temperature values of the thermostatic chambers in top panels were set according to the conditions given in **Table 1**. To realize the developing horizontal convection, denoted as Case D, the temperatures of the top panels, from T_1 to T_4 were set to be higher than the initial temperature T_0, and the image acquisitions were continued until $t = 120$ min (~ 0.4 times of the thermal diffusion time scale) to observe the development of the flow structure. This observation time is sufficiently long to observe the HC development process in a stratified environment while avoiding the initial transient state affected by the experimental constraints. Details concerning this provided later.

A preliminary experiment revealed that the system requires approximately 12 h, corresponding to 2.4 thermal diffusion times, to reach a thermal equilibrium state. Until then, the circulating region formed beneath the top boundary continues to grow slowly towards the bottom of the container with increasing thickness. The development of the circulating region was not complete after one thermal diffusion time; this may be due to the low heat transport efficiency by the horizontally elongated thin layer of circulation. Experimental works by Mulllarney et al. (2004) and Wang & Huang (2005) have also reported very long times (dozens of hours) required to reach thermal equilibrium states; they have observed similar transient processes in their upside-down configurations. Such a very long waiting time is not realistic in a laboratory environment in terms of the homogeneous dispersion of tracer particles. For thermally equilibrated horizontal convection, denoted as Case E, therefore, the average temperature from T_1 to T_4 was set to T_0 and after at least 60 min (assumed to be a sufficiently long waiting time), image acquisition was started. Summarizing the above-mentioned conditions as dimensionless parameters, the bulk Rayleigh number was $Ra = g\beta\Delta\theta W^3/(\kappa\nu) = 2.2 \times 10^8$ for all cases and the initial stratification parameter for the developing cases, $\gamma'_{\mathrm{ini}} = g\beta\gamma[\kappa^{1/2}/(g\beta\Delta\theta)]^{4/3} = 9.4 \times 10^{-3}$. Here, g, W, and γ denote the gravitational acceleration, horizontal length of the fluid layer ($= 4L$), and vertical gradient of the stable temperature stratification, respectively; and β, κ, and ν are the thermal expansion coefficient, thermal diffusivity, and kinematic viscosity, respectively, of the test fluid, distilled water, in the conducted experiment. With these conditions, the flow state is expected to be two-dimensional at least in the developing cases according to our earlier work (Noto et al. 2021).

Thermochromic liquid crystal (TLC, mean diameter of ~15 μm, mean density of 1.02×10^{-3} kg/m^3, KWN-2025 and KWN-2530, Japan Capsular Products Inc.) microcapsules were seeded in degassed water (with a Prandtl number of $Pr = \nu/\kappa = 7$ at $T = 20$°C) as the test fluid for the

temperature and flow visualization. Notice that to cover the wide temperature range in the developing cases, two types of TLC microcapsules with different approximate temperature ranges, 20-25°C (KWN-2025) and 25-30°C (KWN-25-30, were used simultaneously. Since their temperature ranges did not overlap, coloration repeats two color cycles of red, green, and blue from lower to higher temperature. The vertical cross section at the center, $y = 0.5L$, was illuminated using a white light sheet generated by a cylindrical lens and a halogen lamp and photographed using a CMOS color camera (DFK 33UP5000, Imaging Source Co.) with a spatial resolution of 0.083 mm/pixel and a frame rate of 10 frames per second. The thickness of the light sheet was approximately 3–5 mm depending on the distance from the lens. This thickness is however not a problem because a quasi-two-dimensional flow emerged. An example of snapshot images is shown in **Fig. 2(a)** from Case E-1, where the two left panels have higher temperature than the right two panels. Because of the TLC coloration from red to blue for lower to higher temperatures, the region beneath the left panels has bluer colors, which transitions to redder colors from the middle to right regions along the top boundary.

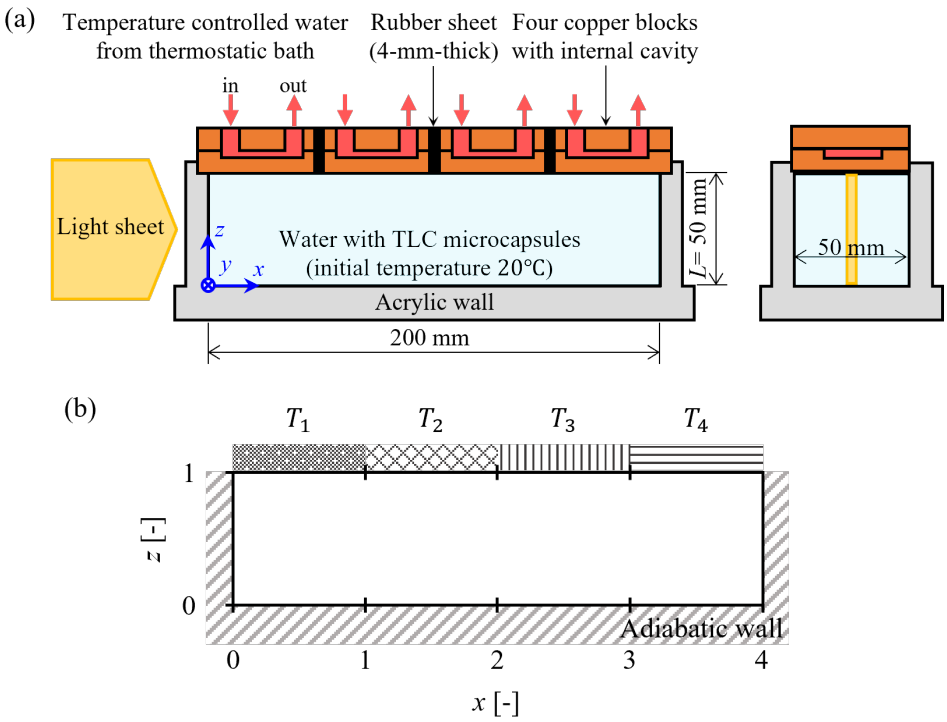

Fig. 1 (a) Schematic diagram of experimental apparatus, and (b) thermal boundary conditions

In this study, the coloration of the TLC microcapsules was only used for a qualitative visualization of the temperature field. Because individual TLC microcapsules particles can be distinguished in the images (see the enlarged image in **Fig. 2(b)**) and because the particles have good traceability in the flow, particle tracking velocimetry (PTV) with the nearest neighbor algorithm was adopted to obtain the velocity vector fields. Numerous velocity vectors obtained via PTV were rearranged in 10-mm-square grids and averaged over time (1 min) and space (grid interval) assuming

gentle and smooth flows to clearly visualize the flow structure. Further details concerning the PTV analysis and post-processing used to obtain the short-time, locally averaged velocity field are given in Noto et al. (2021).

Table 1 Boundary temperature conditions, where the prefix of case number indicate D for "developing" and E for "equilibrium" horizontal convection, respectively. In the former case the lower temperature of top panels is set higher than the initial temperature of the fluid layer, $T_0 = 20$ ˚C, and the latter case it is set lower than T_0.

Case	Arrangement	T_1	T_2	T_3	T_4
D-1	HHLL	26	26	24	24
E-1	HHLL	21	21	19	19
D-2	HLLH	26	24	24	26
E-2	HLLH	21	19	19	21
D-3	LHHL	24	26	26	24
E-3	LHHL	19	21	21	19
D-4	HLHL	26	24	26	24
E-4	HLHL	21	19	21	19

Unit = ˚C

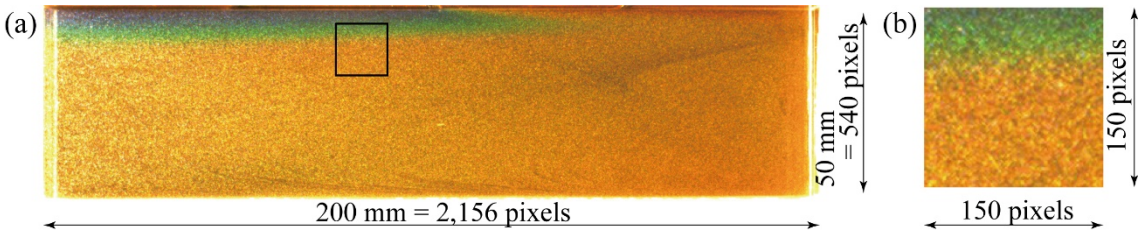

Fig. 2 (a) An example of visualized temperature field by dispersed microcapsules of thermochromic liquid crystal, and (b) an enlarged image extracted from (a) at the square region fringe with black line

3 Visualized convection structures in developing and equilibrium cases

Snapshots of the instantaneous temperature fields visualized using the TLC microcapsules at the different boundary temperature conditions summarized in **Table 1** are shown in **Fig. 3**. In this figure, the left and right panels show the developing and equilibrium conditions, respectively. The difference in the coloration between the conditions occurs because of the relationship between the set temperatures at the top boundary, which are shown schematically in the figure, and the TLC coloration range. The black bands that appear in the images (which are more noticeable in the developing cases) indicate much smaller number of TLC microcapsules. This may be due to the gradual subsidence progress of the microcapsules with advection along the top boundary and to the circulation of that portion of the fluid in the limited thin layer. Corresponding movies of the temperature fields shown in the figure are provided in the supplementary material, where the playback speed of the movies is set to 50 times the recorded speed. Since coloration of the TLC microcapsules depends on angles of the

incident light and the observer, colors shown here do not match completely the temperature ranges of coloration of each type of TLCs. It should be noted that in the movies of developing cases initial bluish regions in the bottom half of the fluid layer exhibit tending to be reddish despite heating on the top plates. This indicates that the temperature range of the bottom region shifts from that of the lower-temperature TLC to that of the higher-temperature TLC, i.e., the bulk temperature increases with time due to the surface heating.

The snapshots confirm the characteristic flow structures in the developing cases, as shown in the left panels in **Fig. 3**. For all heating panel arrangements, shallow circulations emerge beneath the top boundary; however, the number of circulations differs depending on the conditions. In the equilibrium state summarized in the right panels in **Fig. 3**, the circulations are developed and extend throughout the entire fluid layer. The flow structures appear similar to RBC; however, the combination of the horizontal and vertical temperature gradients produces complexity in the structures. In the following subsections averaged velocity vector fields obtained under the different conditions summarized in **Table 1** are shown to investigate the details of the flow structures for the different heating panel arrangements in both the developing and equilibrium cases.

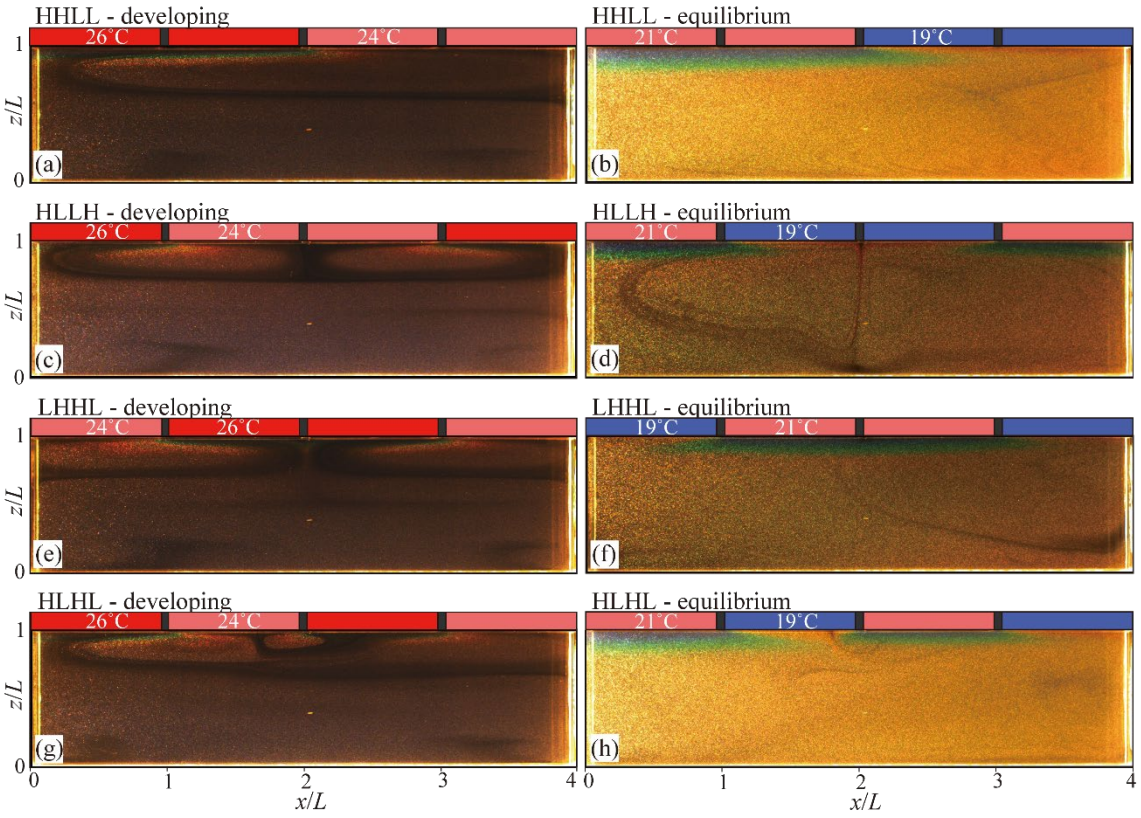

Fig.3 Instantaneous temperature field visualized by TLC microcapsules at different boundary temperature conditions, (a)(b) HHLL, (c)(d) HLLH, (e)(f) LHHL, and (g)(h) HLHL arrangement, where the left and right panels are from different temperature conditions set for developing cases (taken at t = 120 min) and equilibrium states (t = 60 min).

3.1 Developing cases

Details concerning the flow structures formed in the developing cases under different heating panel arrangement conditions are discussed given the averaged velocity vector fields shown in **Fig. 4**. In this figure the averaged velocity vectors are thinned to better visualize the flow structure, and the color represents the local velocity intensity calculated from the vertical and horizontal velocities, u and w, respectively. Averaging in time (1 min) and space (10 mm, the grid interval) does not affect the discussed results because the velocity fields vary smoothly in time and space. It also should be noted that velocity vectors are obtained even in the black band typically observed in the developing cases (**Fig. 3**(a), (c), (e), and (g)). The velocity fields were obtained at t = 120 min from the start of heating. Time variations of the physical variables representing the phenomena shown later indicate that the flows are in the developing stage, as described by the scaling law obtained in a previous study (Noto et al., 2021), at this period beyond the initial transient state.

3.1.1 HHLL arrangement. A horizontally asymmetric arrangement of the heating panels is a typical condition that has been examined in multiple studies (Hughes & Griffiths, 2008). In **Fig. 4(a)**, the flow field in the developing case under the HHLL arrangement condition (Case D-1), where the heating temperature changes at the center, is shown. In this arrangement condition, a large horizontal temperature gradient exists at the center of the top horizontal boundary. Clockwise (CW) baroclinic torque resulting from the horizontal temperature gradient occurs at this location and drives a rightward flow. The flow reaches the right sidewall and moves downward, resulting in a CW circulation flow with the vortex center slightly offset downstream of the horizontal center of the fluid layer at x/L = 2.1. The circulation is localized within the upper region of the fluid layer, because the entire fluid layer is in a stable temperature stratification configuration. The weak flow caused by the baroclinic torque, with a maximum velocity of approximately 0.6 mm/s, cannot penetrate the deeper layer given the buoyancy resulting from the stratification. In addition, the strength of the stable temperature stratification varies in the horizontal direction, and the layer thickness of the circulating flow is larger on the right side, where the stable temperature stratification becomes weaker than it is on the left side. At the bottom of the fluid layer, there is a much weaker circulation driven by the top circulation as a result of the viscosity.

3.1.2 HLLH and LHHL arrangement. The HLLH and LHHL arrangements have opposite heating panels arrangements, with the relatively high (H) and low (L) heating sources being arranged symmetrically with respect to the center of the container. Both arrangements have large horizontal temperature gradients at x/L = 1 and 3, and at these locations, baroclinic torque in different directions act on the fluid beneath the top boundary. The averaged velocity vector fields for these arrangements are shown in **Figs. 4**(b) and 4(c), respectively. Two shallow circulations with opposite rotation emerge beneath the top boundary (Case D-2 and D-3) because of the stable temperature stratification, as

observed in the HHCC arrangement in **Fig. 4(a)**. The circulations have good symmetry in the horizontal plane as well as between the two arrangements. Each circulation is similar to the single circulation observed in **Fig. 4(a),** their similarities being the maximum velocity at the somewhat downstream horizontal positions, the relatively stronger descending flow, and the indistinct ascending flow. The maximum velocities are similar and on the same order as the single shallow circulation shown in **Fig. 4(a)**. This means that the flow velocity is solely determined by the horizontal temperature gradient, not by the arrangement of the panels at least for this aspect ratio of the fluid layer. The thickness of the circulation is, however, considerably smaller in **Figs. 4(b) and 4(c)** than in **Fig. 4(a)**.

3.1.3 HLHL arrangement. In the remaining HLHL arrangement, there are three discontinuous temperature points along the top horizontal plane, and the baroclinic torque drives a flow to the right at $x/L = 1$ and 3 and to the left at $x/L = 2$. As a result, the flow circulates counterclockwise (CCW) in the center of the fluid layer and CW on the two sides. In the developing case (Case D-4, **Fig. 4(d)**), unlike in the HLLH and LHHL arrangement, three closed circulations do not emerge; however, three indistinct circulations are embedded in a single circulation occupying the entire horizontal extent. This is because of the uneven baroclinic torque; the CW circulation is much stronger than the CCW circulation in the fluid layer. The layer thickness of the central circulation is much smaller than that of the circulations on the two sides. The horizontal stream along the top boundary appears to be distorted as well as accelerated by the central circulation. The maximum velocity has a similar value to those of the other arrangements (**Figs. 4(a)–4(c)**).

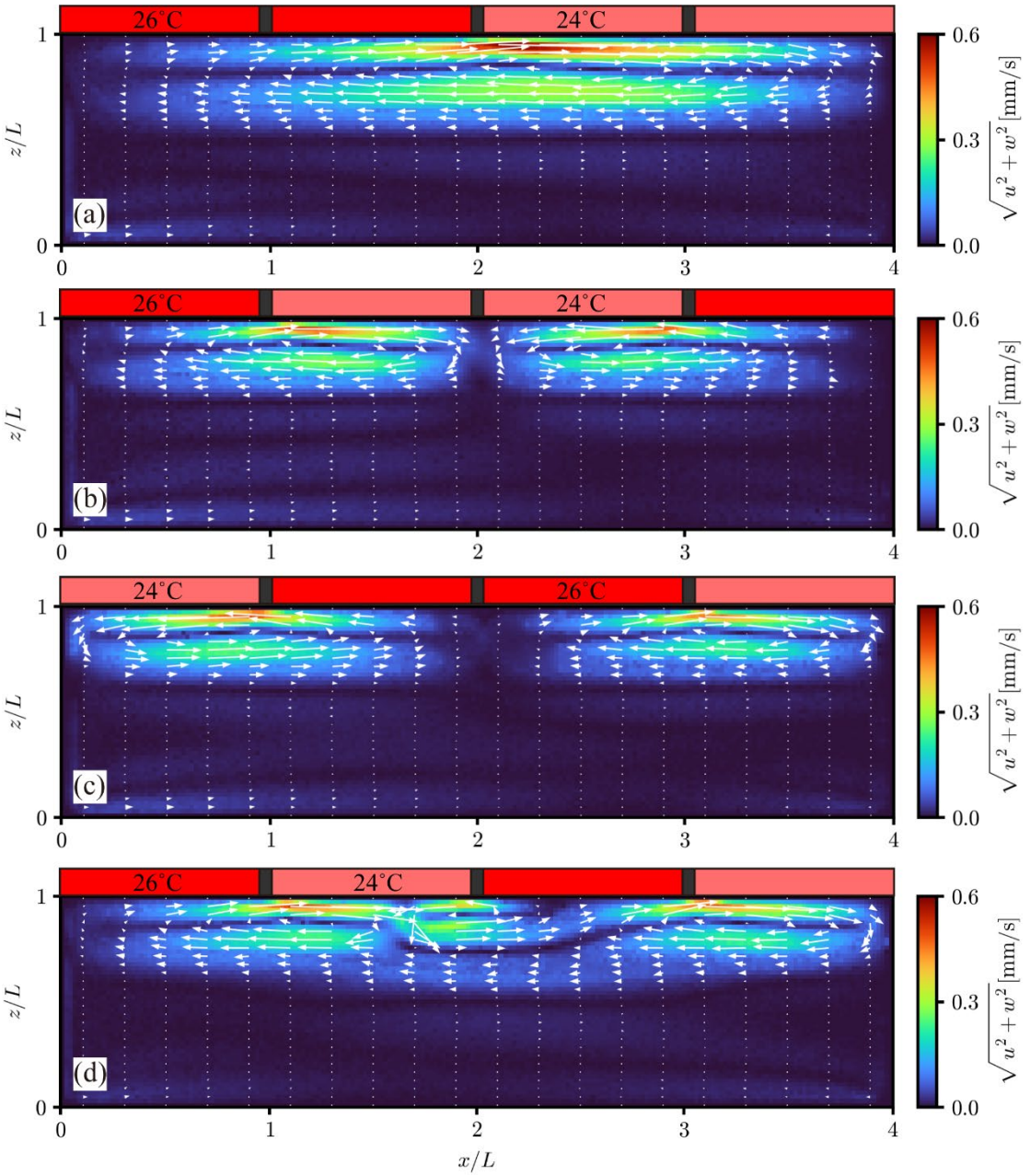

Fig. 4 Averaged velocity vector field and distributions of velocity intensity in developing cases at t = 120 min for the arrangement case of (a) HHLL (Case D-1), (b) HLLH (Case D-2), (c) LHHL (Case D-3), and (d) HLHL (Case D-4). Color contours represent local speeds, and white vectors indicating local velocity vectors are thinned, one tenths and half in the x and z directions, for better visibility. Corresponding temperature fields are given as supplemental movie (**HHLL_D_50x**, **HLLH_D_50x**, **LHHL_D_50x**, and **HLHL_D_50x**).

3.2 Time variations of the flow in the developing cases

The influence of the heating panel arrangement on the averaged velocity fields of the developing cases was discussed in the last section. In this section, the time variations of the flow fields in the developing cases, including those at t = 120 min shown in **Fig. 4**, are investigated. As representative physical

variables describing the flow fields, the time variations of the maximum horizontal speed of the convection, u_{max}, and the thickness of the shallow horizontal stream that emerges beneath the top plate, δ, are shown in **Figs. 5** (a) and **5**(b), respectively. The latter was determined as the vertical distance from the top boundary to the zero-crossing point of u at the location of the large horizontal temperature gradient, namely, $x/L = 2$ for the HHLL condition, $x/L = 1$ for the HLLH, LHHL, and HLHL conditions (denoted HLHL-l), and $x/L = 3$ for the HLHL condition (denoted HLHL-r). Note that the time average for these values does not affect the characteristics of the longtime variation discussed here.

The variations of u_{max} shown in **Fig. 5(a)** indicate two significant characteristics. First, the variations show similar trend and slopes with time regardless of the heating panel conditions. These are initially steeper and become gradual after 30–40 min. In Noto et al. (2021), the influence of the time development is considered via the relaxation of the temperature stratification by evaluating the dimensionless, instantaneous stratification parameter,

$$\gamma' = \frac{g\beta\Delta T_{\mathrm{wall}}}{\sqrt{\kappa t}}\left(\frac{\sqrt{\kappa}}{g\beta\Delta\theta}\right)^{4/3}, \tag{1}$$

where t is the time from the start of heating and, ΔT_{wall} is the initial averaged temperature difference at the top boundary with respect to T_0, where $\Delta T_{\mathrm{wall}} = 5$°C in the present setting. The initial temperature stratification was weakened with time as the gradual increase of the average temperature by the thermal diffusion. Noto et al. (2021) derived scaling law from experimental data, $u_{max} \propto \gamma'^{-0.15}$, which is indicated by the dashed lines in the figure as visual guides. Despite a different heating panel arrangement in Noto et al. (2021), HLLL in the present discretion, the variations obtained in the present experiment indicate similar slope. As a second characteristic, u_{max} is larger for the HHLL condition than for the other conditions. This may be due to differences in the heating length. If we define the Rayleigh number (Ra) adopting the horizontal length of the cells, the convection for this condition has a much larger Ra. The difference in the velocity is, however, not so large, approximately 13%, in comparison with expectations from the usual scaling law, for example, $Ra^{0.5}$. This may suggest that adopting the horizontal length scale to evaluate the Rayleigh number is not suitable to describe the observed phenomena.

The variations of δ also can be separated into two stages, before and after t = 30–40 min, and the latter shows steeper slope. The scaling law, $\delta \propto \gamma'^{-1/4}$, indicated by broken lines in **Fig. 5**(b), was also given in a previous paper (Noto et al., 2021). The present variations seem to take similar slope, after 30–40 min for all heating panel arrangement conditions. Similar to the maximum speed, the variation of δ takes a much larger value for the HHLL condition than for the other conditions. This also supports a reconsideration of the characteristic length. Although acrylic resin adopted in the present setup for surrounding side walls of the fluid layer has small thermal conductivity, there is considerable heat loss through the side walls in such long measurement time, 120 min. The heat loss

has potential to modify the time variation of γ' and relaxation of the temperature stratification would be delayed. The present time variation δ, however, seems to obey quasi-idealized trend about γ'. This suggests no significant influence of the heat loss on the development of horizontal convection.

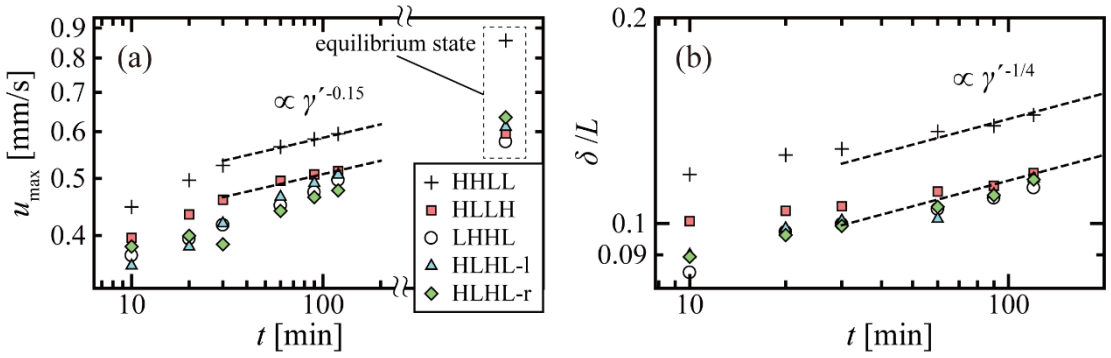

Fig. 5 Time variations of (a) the maximum horizontal speed of the flow, u_{max}, and (b) thickness of the shallow horizontal stream beneath the top boundary, δ in the developing cases for the different heating panel arrangements, where the broken lines indicate guide of power laws derived in the previous work (Noto et al., 2021). Plots at the right side of figure (a) are from the equilibrium state for references.

3.3 Equilibrium cases

The flow structures that formed in the equilibrium cases are detailed in the averaged velocity vector fields shown in **Fig. 6**. These velocity vector fields were obtained for each different heating panel arrangement condition examined in the developing cases, but set temperatures are different from the developing cases. The original velocity vector fields were taken t = 60 min from the start of heating, and the velocity fields did not change significantly after that time. The velocity fields were strongly affected by the vertical temperature gradient, and the range of color bars representing the magnitude of the local velocity intensity differ for each condition.

3.3.1 HHLL arrangement. The flow structure in the thermally equilibrated state under the same arrangement condition (Case E-1) shown in **Fig. 6(a)** changes dramatically with respect to the corresponding developing condition (**Fig. 4(a)**). A strong downward flow along the right wall occurs as a result of the upper cooling. This is because the average temperature in the fluid layer is higher than that of the top panels, T_3 and T_4. A CW circulation therefore forms over the entire layer as expected, and the baroclinic torque works to strengthen this circulation. On the left side, where the fluid layer is in a stable temperature stratification, a broad and gentle upward flow emerges counter to the stronger downward flow. The maximum velocity is further displaced to the right compared with the transient state, and is determined by the balance between the baroclinic torque and the buoyancy resulting from the unstable temperature stratification. The ejection of cold plumes from the top-right corner can be observed in the supplementary movie, even though this feature is obliterated by average in the averaged velocity vector field. The flow is much more unsteady, and the velocity is much greater than in the developing case (see the color bars in **Fig. 4**).

3.3.2 HLLH and LHHL arrangement Unlike the symmetric flow pattern between the HLLH and LHHL arrangements in the developing case (**Figs. 6(b) and 6(c)**), in the equilibrium state (Case E-2 and E-3, respectively) the flow structure shows a distinct difference between these two conditions (**Figs. 4(b) and 4(c)**). In the HLLH arrangement, a strong downward flow, which reaches the bottom wall and rebounds, is driven by the thermal buoyancy at the center (**Fig. 6(b)**). This strong vertical flow may cause oscillatory motions when a stronger baroclinic torque is imposed (Reiter & Shishkina, 2020). Two circulation flows are formed over the entire layer. At x/L = 1 and 3, the baroclinic torque assists the circulations as in **Fig. 4(b)**; however, the most distinct flow is the descending flow at the center not the horizontal flow at the two side points. On the two sides, the upward flows are wide and gentle as a result of the stable temperature stratification compared with the downward flow. In the LHHL arrangement, unlike in the developing case, the flow pattern in **Fig. 6(c)** does not show two distinct circulations. The baroclinic torque and negative temperature gradient on the two sides induce strong corner flows. The returning flow at the center is however indistinct and appears to lose symmetry in the horizontal direction. This is because the descending flows near the sidewalls are influenced by viscous resistance from the sidewalls, and the stable temperature stratification near the center brakes the ascending flow. The maximum velocity is therefore much smaller than that of the descending flow in the HLLH arrangement (**Fig. 4(b)**), as indicated by the color bars in the two figures. The arrangement of the heating panels influences the determination of the flow pattern in the equilibrium condition.

3.3.3 HLHL arrangement. The fluid layer involves unstable temperature stratification in the thermal equilibrium state beneath the second and forth panel from the right side in addition to the baroclinic torque at the three locations of the temperature gradients (Case E-4). The flow patten however cannot achieve individual closed circulation even with the unstable temperature stratification (**Fig. 6(d)**). While retaining a similar flow pattern to that observed in the developing case (**Fig. 4(d)**), the circulation expands throughout the entire fluid layer. This pattern is similar to that of the HHLL arrangement (**Fig. 6(a)**); however, the horizontal streaming along the top boundary is bent and accelerated around x/L = 2 as a result of the baroclinic torque in the CCW direction and the cooling from the top boundary. In comparison with the HHLL arrangement (**Fig. 6(a)**) the maximum velocity is reduced. This may be because the two relatively cool panels separated in the horizontal plane do not provide an effective unstable temperature stratification, especially the second panel. Unlike in the developing case, the downward flow along the right wall resulting from the unstable temperature stratification, which is strong enough to reach the bottom, causes a stronger circulation. This may modify the temperature distribution throughout the entire the fluid layer. It is also possible that the horizontal circulation enhanced by the negative temperature stratification relaxes the horizontal temperature gradient between the H and L heating panels, and that the influence of the baroclinic torque is weakened.

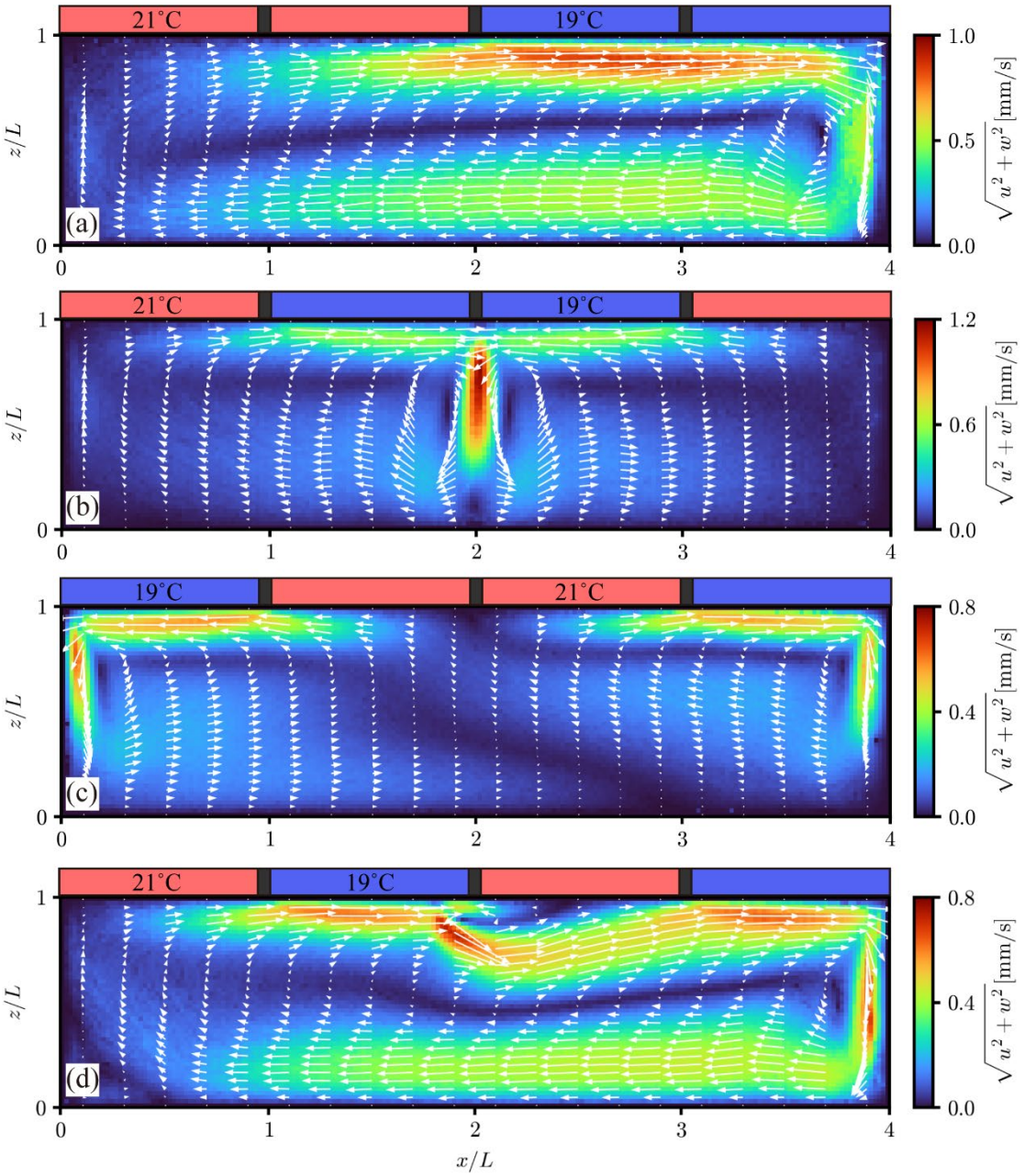

Fig. 6 Averaged velocity vector field and distributions of velocity intensity in equilibrium cases at t = 60 min for the arrangement case of (a) HHLL (Case E-1), (b) HLLH (Case E-2), (c) LHHL (Case E-3), and (d) HLHL (Case E-4). Color contours represent local speeds, and white vectors indicating local velocity vectors are thinned, one tenths and half in the x and z directions, for better visibility. Corresponding temperature fields are given as supplemental movie (**HHLL_E_50x**, **HLLH_E_50x**, **LHHL_E_50x**, and **HLHL_E_50x**).

Conclusions

This study examined the influence of the heating panel arrangement on the formation of flow pattern in developing and thermally equilibrium horizontal convection confined in a rectangular vessel.

Velocity vector field measurement using TLC microcapsules as a flow tracer allowed quantitative flow visualization over a two-hour period. As expected from a previous study (Noto et al., 2021), in the transient state with an initial stable temperature stratification, the flow pattern formed in each arrangement involved shallow circulation beneath the top boundary and the number of circulations along the horizontal direction was determined by the number of points having horizontal temperature gradient (see the schematic illustrations summarized in **Fig. 7**). The maximum velocities induced by the baroclinic torque are nearly the same in all cases, independent of the heating panel arrangement.

The velocity vector measurements also allowed the time development of the flow in the developing cases to be investigated. The time variations of the maximum horizontal speed of the convection and the depth of the shallow horizontal flow that emerged beneath the top boundary calculated from the velocity fields indicate that the variations can be distinguished into the initial transient and developing stages. The latter has similar slopes regardless of the heating panel arrangement conditions and the slopes are close to the scaling law given in a previous study (Noto et al., 2021) despite the different heating panel condition. The scaling law describes the influence of the gradual relaxation of the stable temperature stratification. In addition, the results indicate that the values cannot be organized into scaling laws using the horizontal length scales of the panels or the circulations as the characteristic length.

To achieve the equilibrium state with a shorter time, we set the average temperature of the heating panels to be the same as the initial temperature of the fluid layer. The flow pattern observed under this condition indicated that the flow pattern is strongly influenced by the arrangement of the heating panel in the equilibrium state (see the schematic illustrations summarized in **Fig. 7**). This is because the unstable temperature stratification formed in the equilibrium state dominates the flow pattern and modifies the temperature distribution, and because the baroclinic torque is not already dominant such that it can determine the flow pattern.

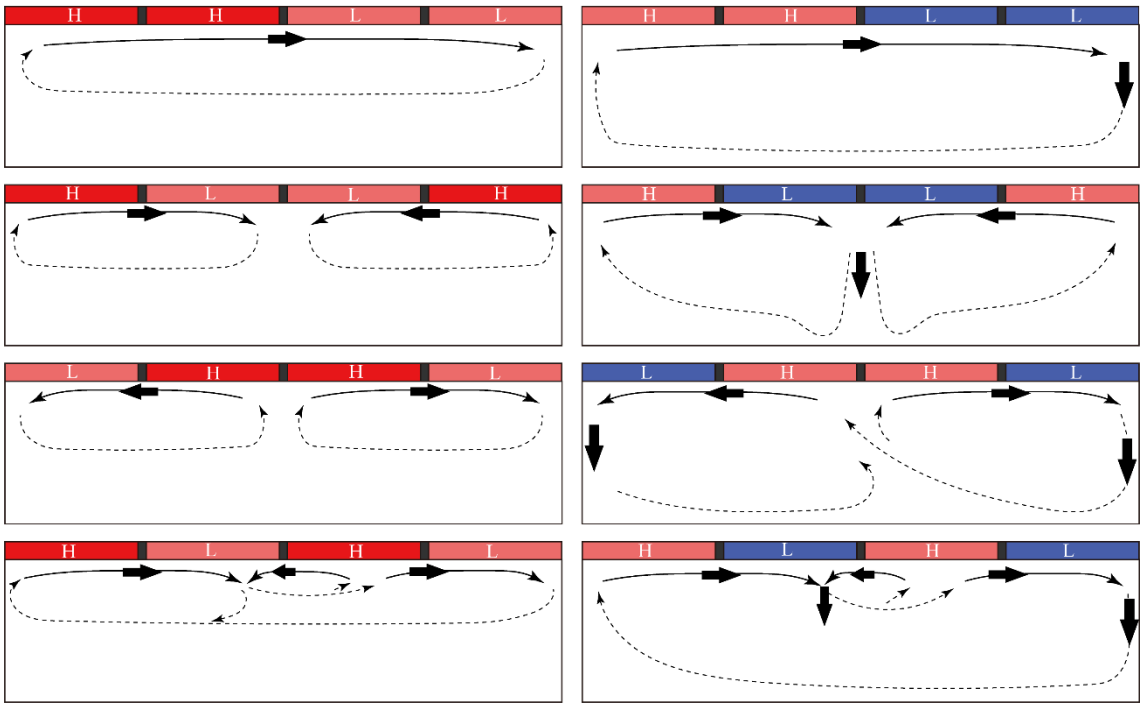

Fig. 7 Schematic illustration of flow patterns observed at different thermal boundary conditions, where the left and right panels are for developing and equilibrium cases Symbols of H and L on the top boundaries denote relatively hot and cold thermal conditions, respectively. Black arrows indicate the directions of driving force, baroclinic torque due to horizontal temperature gradient and buoyancy due to unstable temperature stratification.

Acknowledgement

The authors are grateful for a financial support obtained through a Grant-in-Aid for Japan Society for Promotion of Science Fellows (Grant No. JP19J20096).

References

Chiu-Webster, S., Hinch, E. J., & Lister, J. R. (2008). Very viscous horizontal convection. Journal of Fluid Mechanics, 611, 395-426.

Coman, M. A., Griffiths, R. W., & Hughes, G. O. (2006). Sandströms experiments revisited. Journal of Marine Research, 64(6), 783-796.

Gayen, B., Griffiths, R. W., Hughes, G. O., & Saenz, J. A. (2013). Energetics of horizontal convection. Journal of Fluid Mechanics, 716.

Gramberg, H. J. J., Howell, P. D., & Ockendon, J. R. (2007). Convection by a horizontal thermal gradient. Journal of Fluid Mechanics, 586, 41-57.

Griffiths, R. W., Hughes, G. O., & Gayen, B. (2013). Horizontal convection dynamics: insights from transient adjustment. Journal of Fluid Mechanics, 726, 559-595.

Lu, J., Arya, S. P., Snyder, W. H., & Lawson Jr, R. E. (1997). A laboratory study of the urban heat island in a calm and stably stratified environment. Part I: Temperature field. Journal of Applied Meteorology, 36(10), 1377-1391.

Hughes, G. O., & Griffiths, R. W. (2008). Horizontal convection. Annu. Rev. Fluid Mech., 40, 185-208.

Mori, A., & Niino, H. (2002). Time evolution of nonlinear horizontal convection: Its flow regimes and self-similar solutions. Journal of the atmospheric sciences, 59(11), 1841-1856.
Mullarney, J. C., Griffiths, R. W., & Hughes, G. O. (2004). Convection driven by differential heating at a horizontal boundary. Journal of Fluid Mechanics, 516, 181-209.
Noto, D., Terada, T., Yanagisawa, T., Miyagoshi, T., & Tasaka, Y. (2021). Developing horizontal convection against stable temperature stratification in a rectangular container. Physical Review Fluids, 6(8), 083501.
Reiter, P., & Shishkina, O. (2020). Classical and symmetrical horizontal convection: detaching plumes and oscillations. Journal of Fluid Mechanics, 892, R1.
Rossby, H. T. (1965, February). On thermal convection driven by non-uniform heating from below: an experimental study. In Deep Sea Research and Oceanographic Abstracts (Vol. 12, No. 1, pp. 9-16). Elsevier.
Ulloa, H. N., Ramón, C. L., Doda, T., Wüest, A., & Bouffard, D. (2022). Development of overturning circulation in sloping waterbodies due to surface cooling. Journal of Fluid Mechanics, 930.
Wang, W., & Huang, R. X. (2005). An experimental study on thermal circulation driven by horizontal differential heating. Journal of Fluid Mechanics, 540, 49-73.